

Anomalous Rainfall over Southwest Western Australia Forced by Indian Ocean Sea Surface Temperatures

CAROLINE C. UMMENHOFER AND ALEXANDER SEN GUPTA

Climate Change Research Centre, University of New South Wales, Sydney, New South Wales, Australia

MICHAEL J. POOK

Centre for Australian Weather and Climate Research, CSIRO, Hobart, Tasmania, Australia

MATTHEW H. ENGLAND

Climate Change Research Centre, University of New South Wales, Sydney, New South Wales, Australia

(Manuscript received 11 September 2007, in final form 19 December 2007)

ABSTRACT

The potential impact of Indian Ocean sea surface temperature (SST) anomalies in modulating midlatitude precipitation across southern and western regions of Australia is assessed in a series of atmospheric general circulation model (AGCM) simulations. Two sets of AGCM integrations forced with a seasonally evolving characteristic dipole pattern in Indian Ocean SST consistent with observed “dry year” (P_{DRY}) and “wet year” (P_{WET}) signatures are shown to induce precipitation changes across western regions of Australia. Over Western Australia, a significant shift occurs in the winter and annual rainfall frequency with the distribution becoming skewed toward less (more) rainfall for the P_{DRY} (P_{WET}) SST pattern. For southwest Western Australia (SWWA), this shift primarily is due to the large-scale stable precipitation. Convective precipitation actually increases in the P_{DRY} case over SWWA forced by local positive SST anomalies. A mechanism for the large-scale rainfall shifts is proposed, by which the SST anomalies induce a reorganization of the large-scale atmospheric circulation across the Indian Ocean basin. Thickness (1000–500 hPa) anomalies develop in the atmosphere mirroring the sign and position of the underlying SST anomalies. This leads to a weakening (strengthening) of the meridional thickness gradient and the subtropical jet during the austral winter in P_{DRY} (P_{WET}). The subsequent easterly offshore (westerly onshore) anomaly in the thermal wind over southern regions of Australia, along with a decrease (increase) in baroclinicity, results in the lower (higher) levels of large-scale stable precipitation. Variations in the vertical thermal structure of the atmosphere overlying the SST anomalies favor localized increased convective activity in P_{DRY} because of differential temperature lapse rates. In contrast, enhanced widespread ascent of moist air masses associated with frontal movement in P_{WET} accounts for a significant increase in rainfall in that ensemble set.

1. Introduction

The seasonal to interannual variability in precipitation in the midlatitudes is generally assumed to be predominantly driven by internal atmospheric dynamics. In contrast to the strong air–sea coupling in the tropics, the ocean’s role in forcing extratropical atmospheric variability is often regarded to be of minor importance.

Kushnir et al. (2002) review the present understanding of the extratropical ocean’s role in modulating atmospheric circulation. They find that in addition to a direct thermal response in the atmospheric boundary layer to sea surface temperature (SST) anomalies, there is also evidence for a significant modulation of the large-scale atmospheric circulation. However, relative to the atmosphere’s internal variability the ocean-induced changes are small. Nevertheless, a wealth of studies have been inspired by the possibility of utilizing the longer persistence of anomalies in the ocean, which in turn might modulate extratropical atmospheric variability, for improving seasonal to interannual climate forecasts

Corresponding author address: Caroline Ummenhofer, Climate Change Research Centre, School of Mathematics and Statistics, University of New South Wales, Sydney, NSW 2052, Australia.
E-mail: c.ummehofer@unsw.edu.au

(Kushnir et al. 2002, and references therein). A few of these studies show clear evidence that the extratropical ocean has a major effect on the large-scale atmospheric circulation (e.g., Czaja and Frankignoul 1999; Rodwell et al. 1999; Sterl and Hazeleger 2005). Many more studies demonstrate the overriding importance of the atmosphere's internal variability, particularly in controlling precipitation on interannual to seasonal time scales (e.g., Harzallah and Sadourny 1995; Rowell 1998; Watterson 2001). There is general agreement that a marked contrast exists between the tropics, where 60%–80% of climate variability is SST forced, and the midlatitudes, where only about 20% can be attributed to SST forcing (Kushnir et al. 2002). In this study, we present evidence for regional midlatitude precipitation being significantly affected by extratropical SST on seasonal to interannual time scales in an atmospheric general circulation model (AGCM). This study is motivated by previous observational and modeling work by England et al. (2006), who find that precipitation over southwest Western Australia (SWWA) can be linked to a recurring SST dipole pattern in the Indian Ocean.

The first proposed link between Australian rainfall variability and SST was made by Priestley and Troup (1966) and further explored by Streten (1981, 1983). Nicholls (1989) describes a gradient in SST between the Indonesian region and the central Indian Ocean that is highly correlated with winter rainfall, extending from the northwest to the southeast of Australia. However, he cautioned against assuming causality, that is, that the SST pattern was *forcing* the rainfall changes. To determine whether SST anomalies could be regarded as the *cause* of rainfall variations, Voice and Hunt (1984) carried out AGCM experiments where the atmosphere was forced by SST anomalies similar to those found by Streten (1981, 1983). However, they find conflicting results, especially in the southern regions of Australia. Frederiksen et al. (1999) use multidecadal AGCM simulations forced with observed global SST to split the rainfall variance over Australia into components resulting from SST forcing and internal variability. In their experiments, the SST forcing seems to be most influential over the tropical northern part of the country. Ansell et al. (2000) find that observed rainfall in southern regions of Australia has a stronger link with variations in mean sea level pressure (MSLP) than with Indian Ocean SST. However, Frederiksen and Balgovind (1994) use an enhanced SST gradient reminiscent of the one described by Nicholls (1989) in AGCM simulations and record an increased frequency of northwest cloud bands and associated winter rainfall over an area extending from the northwest to the southeast of the country. For similar regions over Australia, Ashok et

al. (2003) link positive Indian Ocean dipole (IOD) events with a reduction in winter rainfall leading to a baroclinic response in the atmosphere resulting in anomalous subsidence. Applying an enhanced meridional SST gradient in the eastern Indian Ocean, Frederiksen and Frederiksen (1996) demonstrate an equatorward shift of storm-track instability modes over the Australian region and an increase in the baroclinicity.

For SWWA, Smith et al. (2000) find neither Indian Ocean SST nor MSLP to be closely linked with observed interannual rainfall variability (though they propose that both play a role in long-term trends in the region). More recently, England et al. (2006) identify a characteristic SST pattern and a reorganization of the large-scale wind field over the Indian Ocean region associated with anomalous rainfall years in SWWA in both observations and a multicentury coupled climate model simulation. They find dry (wet) years in SWWA associated with cold (warm) SST anomalies in the eastern Indian Ocean off the northwest shelf of Australia and warm (cold) anomalies in the subtropical Indian Ocean. Concurrently, an acceleration (deceleration) of the anticyclonic basin-wide wind field exists with anomalous offshore (onshore) moisture advection over SWWA. However, it could not be conclusively demonstrated that the SST anomalies were forcing the SWWA rainfall anomalies, or were just symptomatic of the changed wind field. In this latter case, the wind field changes would be the primary cause of both the precipitation and SST anomalies (for SST, air–sea heat flux anomalies would also play a role). The goal of this study is to address the question of whether the SST patterns described by England et al. (2006) are capable of driving SWWA precipitation anomalies using an ensemble set of AGCM simulations.

SWWA is characterized by a Mediterranean-type climate dominated by wet winters and dry summers (Drosowsky 1993). During summer, the influence of the subtropical high pressure belt dominates over this region. The axis of the subtropical ridge moves equatorward in autumn and is located near the northern boundary of SWWA (approximately 30°S) during the winter months (Gentilli 1972). As a consequence, moist westerly winds prevail over SWWA from late autumn into spring. Rainfall associated with the maritime westerlies is enhanced by topography and by the regular passage of cold fronts and associated depressions (e.g., Gentilli 1972; Wright 1974; IOCI 2001). There is a general decrease in rainfall rate from south to north over the SWWA region, but rainfall increases slightly from west to east across the coastal plain, before declining steadily inland of the Darling Scarp (Wright 1974).

SWWA and its surroundings maintain a considerable

proportion of Australia's agricultural production, which is heavily dependent on the winter rainfall. Since the 1970s, a dramatic decrease of about 20% has occurred in autumn and early winter rainfall. This is associated with an even bigger (about 40%) drop in stream inflow into dams (IOCI 2001). The rainfall decline in SWWA, which is the topic of many observational and modeling studies, has been linked to changes in large-scale MSLP (Allan and Haylock 1993; IOCI 2001), shifts in synoptic systems (Hope et al. 2006), changes in baroclinicity (Frederiksen and Frederiksen 2005, 2007), the Southern Annular Mode (Li et al. 2005; Cai and Cowan 2006; Li 2007), land cover changes (Pitman et al. 2004; Timbal and Arblaster 2006), and anthropogenic forcing (Cai and Cowan 2006; Timbal et al. 2006), among others, with a combination of several factors most likely playing a role. In light of these exacerbated conditions and the need for difficult water management decisions, a better understanding of seasonal to interannual rainfall variability in the region is imperative. This is particularly the case because traditional Australian predictors for rainfall variability, such as the Southern Oscillation index, have very limited skill over SWWA (Smith et al. 2000; IOCI 2001). Improvements in seasonal rainfall forecasting, as provided potentially by the greater persistence of oceanic versus atmospheric precursors, could therefore prove valuable.

The existence of Indian Ocean precursors for seasonal forecasting of Australian climate has been proposed in previous studies. Ashok et al. (2003) suggest that links between the IOD and anomalous rainfall in affected regions could help improve predictions in those areas. To improve seasonal forecasts for better agricultural management in a southeastern Australian cropping region, McIntosh et al. (2007) incorporate information on the combined states of the IOD and El Niño–Southern Oscillation (ENSO). The only skillful forecast application of the ENSO–IOD configuration they found is in the transition from an El Niño with positive IOD phase (e.g., in 2006), which gives an approximately 90% likelihood of moving to a more favorable rainfall pattern over southeastern Australia in the following year (Peter McIntosh 2007, personal communication). In a coupled general circulation model simulation, Watterson (2001) finds that the wind anomalies driving rainfall variability over Australia are not associated with any long-term oceanic precursor. Accordingly, he argues, little predictability can be gained from SST–rainfall relationships, because rainfall in Australia is, excepting associations with ENSO, not forced by SST (Watterson 2001). In this study, using AGCM simulations, we will show that Indian Ocean SST

anomalies can indeed give rise to changed thermal properties in the atmosphere, modulate the large-scale atmospheric circulation, and thus ultimately cause precipitation changes on seasonal to interannual time scales. AGCM simulations forced by SST anomalies that are representative of a dry (wet)-case scenario for SWWA allow us to identify causative links that might not be possible using correlation analyses alone.

The remainder of the paper is structured as follows: In section 2, the reanalysis data and the climate model are described, as is the experimental setup and the statistical techniques for analyzing the model output. Section 3 provides an assessment of the suitability of the model for the present study. Section 4 describes the seasonal evolution of SST anomalies used in the perturbation experiments. The induced changes in precipitation in the experiments are presented in section 5. In section 6, changes in thermal properties of the atmosphere and circulation anomalies forced by the perturbations are described, and a mechanism is proposed, explaining the shifts in the rainfall distribution. Section 7 summarizes the findings.

2. Data and data analysis

a. Reanalysis data

To assess the model's suitability for the present study, long-term mean fields in the model are compared to observations across the region for sea level pressure (SLP), surface winds, atmospheric thickness, and precipitation. Data from the 40-yr European Centre for Medium-Range Weather Forecasts (ECMWF) Re-Analysis (ERA-40) at a 2.5° latitude–longitude resolution is used for monthly SLP and surface wind fields for the 1960–2001 period (Uppala et al. 2005). The performance of the ECMWF operational forecasts over the Indian Ocean region is assessed by Nagarajan and Aiyyer (2004). The thickness data for 1000–500 hPa and total and convective precipitation are taken from the National Centers for Environmental Prediction–National Center for Atmospheric Research (NCEP–NCAR) reanalysis (NNR; Kalnay et al. 1996; Kistler et al. 2001) for the same period of 1960–2001. The large-scale monthly precipitation data are taken from the Climate Prediction Center (CPC) Merged Analysis of Precipitation (CMAP; Xie and Arkin 1996) climatology at a 2.5° latitude–longitude resolution for the 1979–2001 period. It combines several diverse datasets, including gauge-based analyses from the Global Precipitation Climatology Center, predictions by the operational forecast model of ECMWF, and three types of satellite estimates. Across the Australian continent, precipitation observations are based on the

gridded SILO data produced by the Australian Bureau of Meteorology with 0.5° latitude–longitude resolution described in detail by Jeffrey et al. (2001).

b. Climate model

The climate model used for our experiments is the NCAR Community Climate System Model, version 3 (CCSM3), run in uncoupled atmosphere-only mode. The atmospheric component of CCSM3, the Community Atmosphere Model, version 3 (CAM3), uses a spectral dynamical core, a T42 horizontal resolution (approximately 2.8° latitude–longitude), and 26 vertical levels. The CCSM3 model, and its components and configurations are described in Collins et al. (2006), with more CAM3-specific details described in Hurrell et al. (2006). Several studies assess the model's performance and suitability for applications in climate research relevant for the present study, in particular, in regard to the representation of the hydrological cycle (Hack et al. 2006), tropical Pacific climate variability (Deser et al. 2006), ENSO variability (Zelle et al. 2005), and monsoon regimes (Meehl et al. 2006). Several biases in the model have been documented, most notably those associated with the tropical Pacific climate, that is, the intertropical convergence zone (ITCZ), South Pacific convergence zone (SPCZ; e.g., Zhang and Wang 2006), and ENSO spatial and temporal variability (e.g., Deser et al. 2006). These issues will be revisited and assessed in the context of this study in section 3a.

c. Experimental setup

The perturbation experiments were conducted using the NCAR CCSM3 run with the monthly SST climatology after Hurrell et al. (2006), which is based on Reynolds SST (Smith and Reynolds 2003, 2004) and Hadley Centre anomalies (Rayner et al. 2003). An 80-yr integration forced by the 12-month climatology was taken as the control experiment (CNTRL). Two sets of perturbation experiments were carried out where anomalous SST patterns were superimposed onto the climatology. These perturbations were derived from composites of observed average monthly SST anomalies for years defined as being extremely dry/wet over SWWA (30° – 35° S, 115° – 120° E) by England et al. (2006), that is, exceeding ± 1 standard deviation in their rainfall time series. Because of the expectation that the resultant atmospheric response would be small compared to the natural variability, the anomalies of England et al. (2006) were scaled by a factor of 3. Scaling the composite SST pattern by this factor more closely represents the magnitude of SST anomalies encountered during any particular extreme year (for de-

tails, see section 4, cf. Figs. 1, 2). The seasonal evolution of the SST anomalies thus derived for the perturbed dry-year case (P_{DRY}) is shown as an example in Fig. 1. No perturbations are applied outside the Indian Ocean domain, that is, the magnitude of the SST anomalies is zero there, as seen in Fig. 1. Though not an exact mirror image of P_{DRY} , anomalies for the wet-year case (P_{WET} ; figure not shown) demonstrate the same general features of the opposite polarity. Perturbation runs were started from a variety of years spanning the control run and integrated from the start of January for one year. The ensemble set consisted of 60 positive and 60 negative 1-yr integrations.

d. Data analysis and statistical methods

For the purposes of our analysis, two regions are defined over which climate variables are averaged. The first represents SWWA, delimited by lines of latitude and longitude at 30° S, 35° S, 115° E, and 120° E (as indicated in Fig. 4c). This limited region contains 11×11 observational and 3×3 model grid boxes. A second region more broadly representative of the subtropical area of Western Australia (WA) is delimited by lines of latitude and longitude at 21° – 35° S, 115° – 130° E (this larger area contains 6×6 model grid points; see Fig. 4d). The tropical north of WA is excluded for the analysis, because it is characterized by a very different rainfall regime dominated by summer monsoons.

The nonparametric Mann–Whitney rank test is used to determine the significance level at which the rainfall frequency distribution in a particular region (SWWA and WA) in the perturbed cases differs from the control (von Storch and Zwiers 1999). Throughout the study, we use a two-tailed t test to determine the significance of the spatial anomaly fields. This test estimates the statistical significance at which the anomalies in P_{DRY} and P_{WET} are distinguishable from the CNTRL at each grid point.

3. Model validation and assessment

a. Atmospheric circulation

To assess the suitability of the model for the present study, the mean annual and seasonal states of key atmospheric variables across the Indian Ocean region are compared between the observations and the model. Annual SLP, surface winds, and thickness are shown in Fig. 3. Seasonal long-term means of these variables were also evaluated and generally demonstrated good qualitative agreement with observations (figures not shown).

The long-term annual mean SLP field in the model

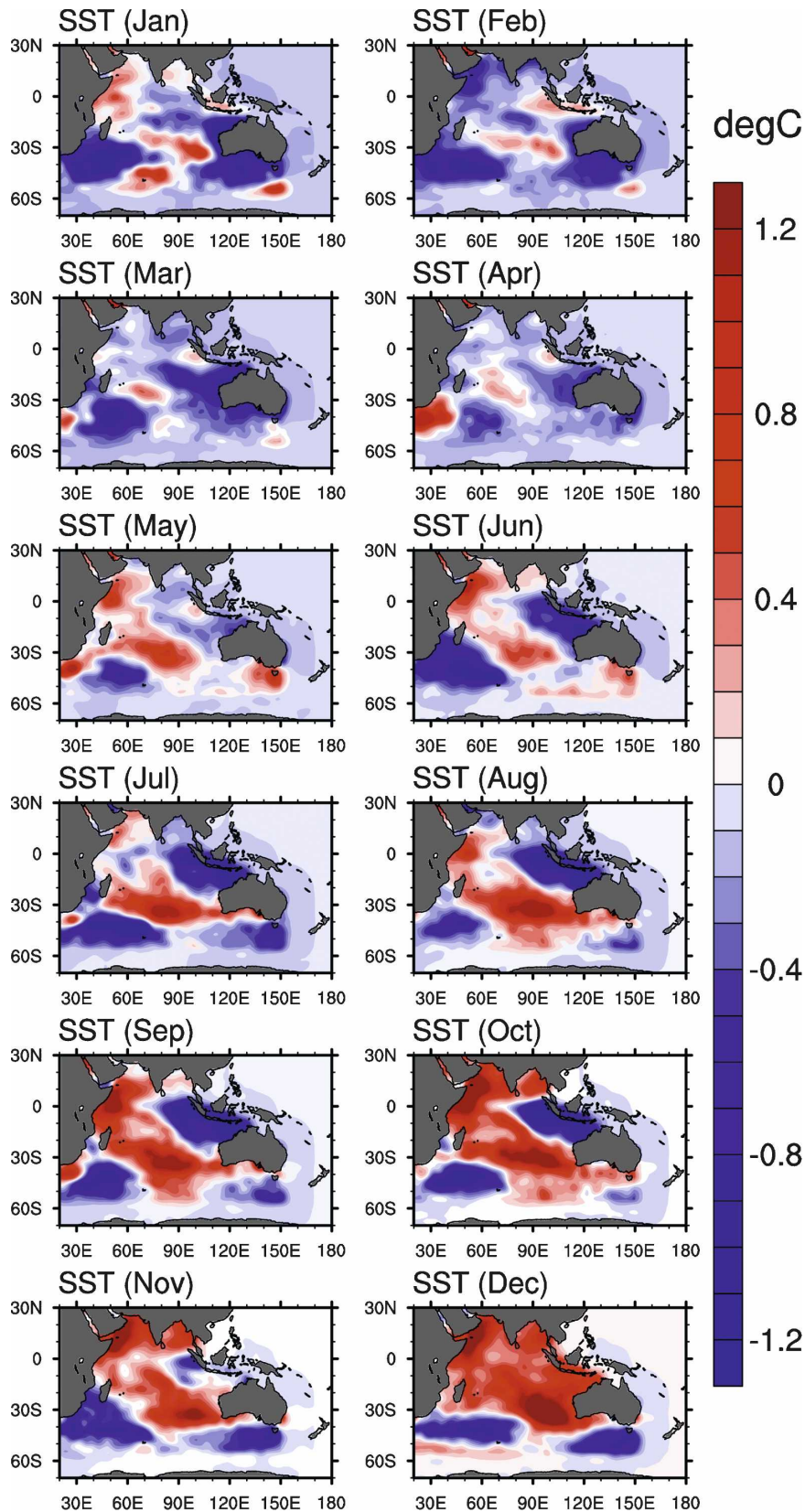


FIG. 1. Monthly SST anomaly ($^{\circ}\text{C}$) superimposed as a perturbation on the climatological SST in the dry-year case (P_{DRY}). Perturbation values outside the Indian Ocean domain are set to zero, that is, forcing in those regions simply follows the climatological SST.

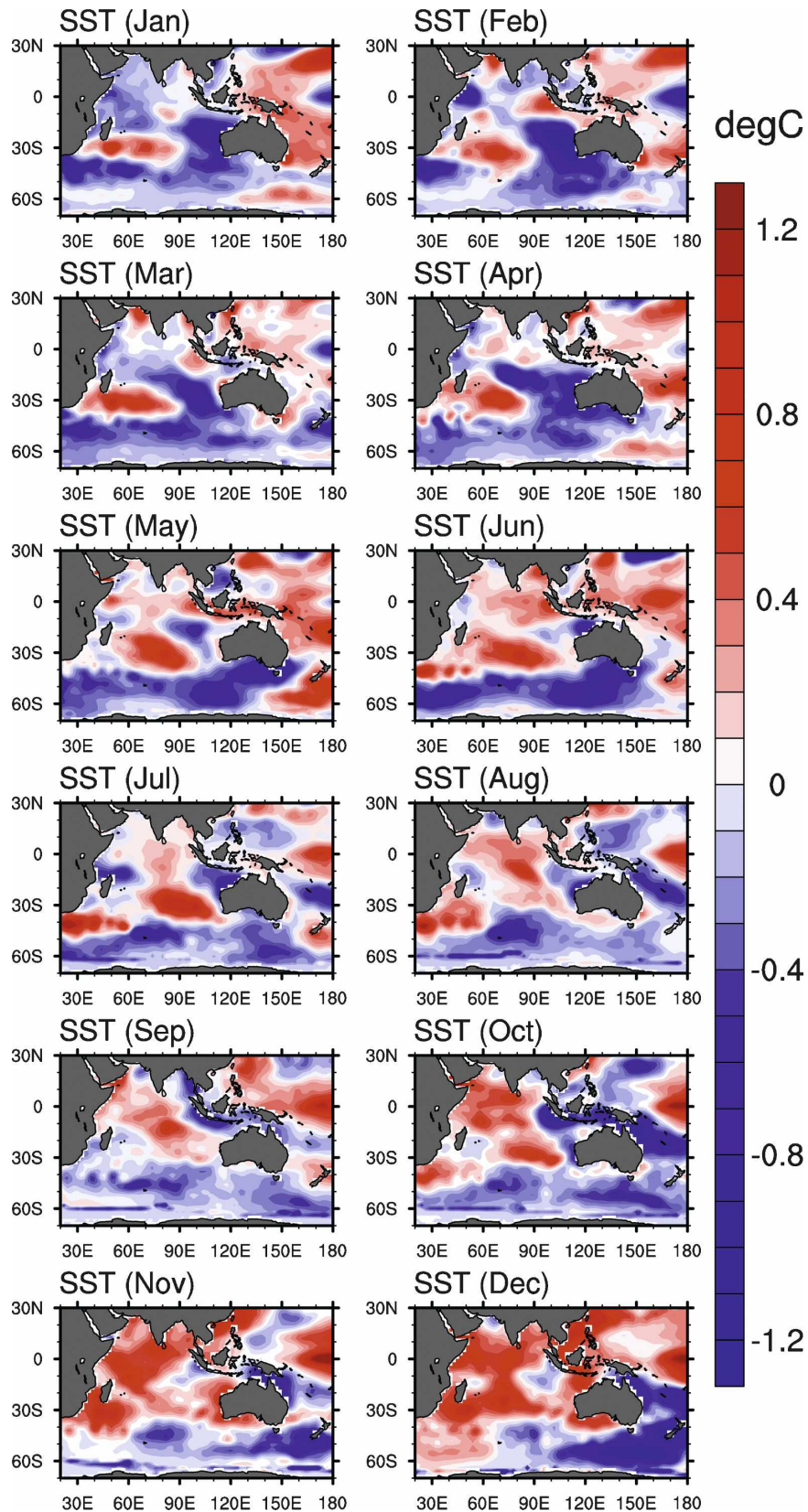


FIG. 2. Observed monthly SST anomaly ($^{\circ}\text{C}$) during 2006, which was a dry year in SWWA.

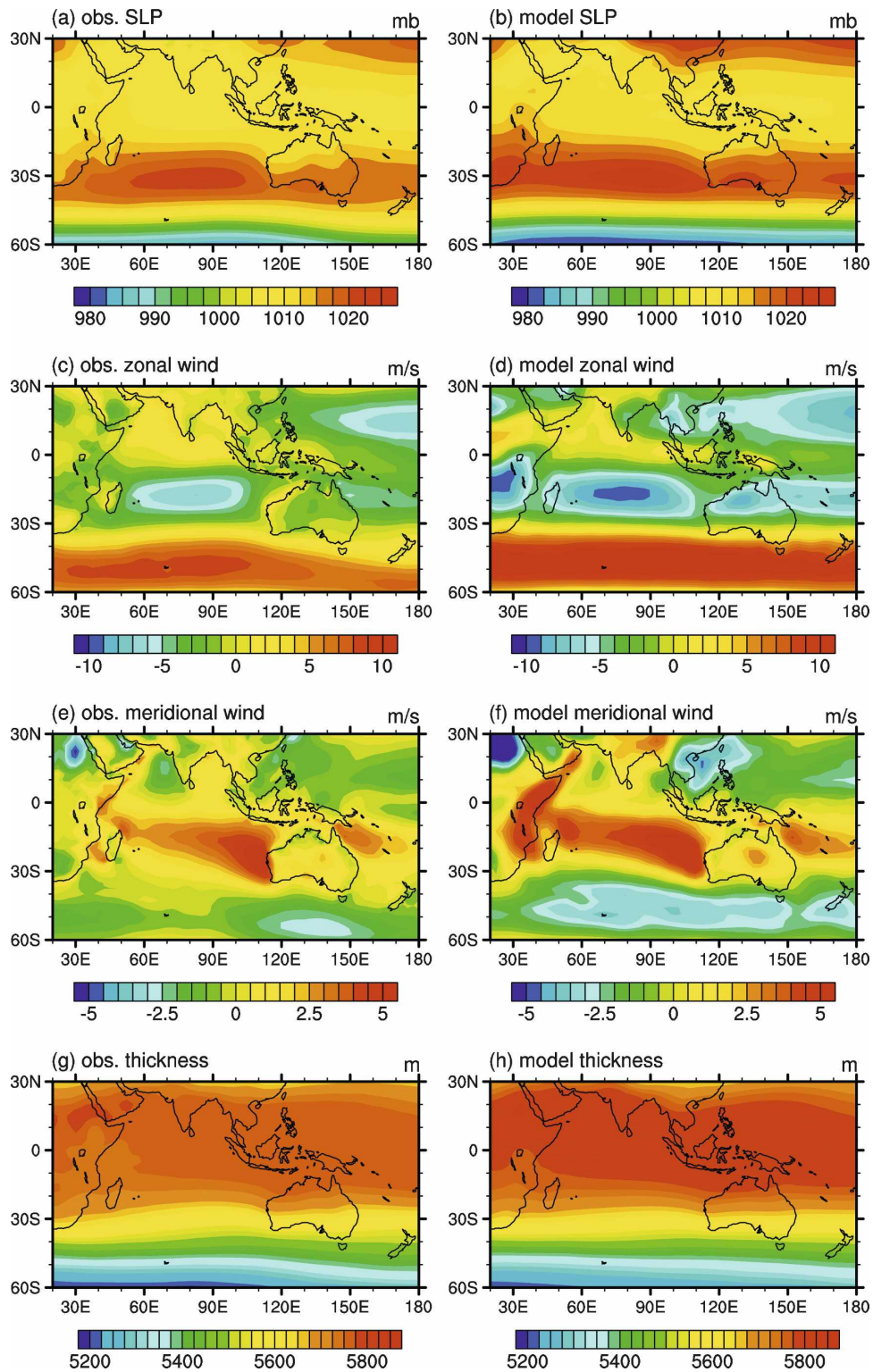


FIG. 3. Annual long-term mean of (a), (b) SLP (mb), (c), (d) zonal, and (e), (f) meridional wind (m s^{-1}), and (g), (h) thickness (m for 1000–500 hPa) fields: (left) observations and (right) model. The long-term mean in the observations is based on ERA-40 (thickness on NNR) data for the 1960–2001 period, the model fields on the 80-yr control run.

captures the overall Southern Hemisphere patterns with a distinct meridional SLP gradient (Figs. 3a,b). However, the pattern is overly zonally symmetric (across all seasons) in the midlatitudes compared to the observations (Sen Gupta and England 2006), resulting in an exaggerated meridional SLP gradient (Hurrell et al. 2006). The seasonal cycle in the movement of the subtropical high pressure belt and the circumpolar trough agrees well with observations, though the latter is too deep and positioned too far equatorward in winter (Hurrell et al. 2006). The overall pattern of subtropical easterlies and midlatitude westerlies at the surface across the Indian Ocean region is captured in the model (Figs. 3c,d). However, as before, the zonal component in the model is slightly overestimated, with a positive bias in the midlatitude westerlies for the latitude band of 35° – 60° S compared to the observations, especially south of Australia and toward New Zealand (Hurrell et al. 2006), and an overly strong easterly wind field across the central Indian Ocean, over northern parts of Australia and extending eastward. In the subtropical easterlies this is especially apparent in the winter half of the year (figure not shown). The meridional wind field in the model closely matches the observations (Figs. 3e,f), with only a slightly enhanced northerly (southerly) component in the latitude band of 40° – 60° S (along eastern Africa). The observed seasonal cycle of strengthening southerly winds across much of the Indian Ocean during the winter months is also well represented in the model (figure not shown). The meridional gradient in thickness is captured very well by the model, and the differences to the observations are small (Figs. 3g,h).

Several biases in the model have been documented previously; most notably, there is a spurious second ITCZ south of the equator in the Pacific and hence a poor simulation of the SPCZ (Zhang and Wang 2006). This is a problem common to many atmospheric general circulation models (Meehl and Arblaster 1998; Hurrell et al. 2006). The positive bias in the tropical Pacific rainfall in both branches of the ITCZ signifies an overly vigorous hydrological cycle there (Collins et al. 2006). The double-ITCZ problem has been linked to a bias in SST in the equatorial Pacific region (Arblaster et al. 2002; Zhang and Wang 2006). This relates to the spatial pattern of ENSO in the coupled model extending too far west in the Pacific Ocean and being too narrowly confined to the equator (Deser et al. 2006). In the atmosphere-only mode, these biases are less pronounced and Deser et al. (2006) speculate that they contribute to the ENSO frequency in the coupled model being too high (2–2.5 yr; e.g., Collins et al. 2006; Deser et al. 2006) relative to the observed frequencies

(3–8 yr; e.g., Kiehl and Gent 2004; Zelle et al. 2005; Collins et al. 2006). So, for the scope of the present study and considering our focus on Indian Ocean variability, the general structure and variability in the tropical Pacific is sufficiently well captured by the model.

b. Precipitation

In Fig. 4, the model precipitation across the Indian Ocean basin is compared to observed estimates based on CMAP data (Xie and Arkin 1996). Because climatologies of observed rainfall differ considerably on both regional and local scales, differences to the model should be taken as qualitative only (Hurrell et al. 2006). The model represents broad patterns of annual mean precipitation across the Indian Ocean basin well, with increased rainfall in the tropics and lower rainfall in the region of the subtropical high pressure belt across the eastern Indian Ocean and over Australia, as well as Africa (Figs. 4a,b). However, the model shows excessive rainfall over the Indonesian Archipelago and the Bay of Bengal compared to the observations, because the tropical maximum remains north of the equator throughout the year (Hurrell et al. 2006). In contrast, the high-rainfall region in the central equatorial Indian Ocean receives too little rainfall. The latter discrepancy is associated with the simulation of a double ITCZ, that is, the persistence of ITCZ-like precipitation north of the equator throughout the year (Hack et al. 2006), which is a problem common to many general circulation models (e.g., Meehl and Arblaster 1998; Hurrell et al. 2006; Zhang and Wang 2006; Zhang et al. 2007). The low-rainfall region in the eastern subtropical Indian Ocean is too dry in the model to the west of Australia, while south of 40° S the model is too wet across the entire Indian Ocean basin compared to the observations, related to a positive bias poleward of the extratropical storm tracks (Hack et al. 2006). Meehl et al. (2006) assess the seasonally varying rainfall associated with monsoonal regimes across the tropical Indian Ocean in CCSM3 in detail. They find the major monsoonal wind features and associated precipitation maxima to be well simulated in the model. Future work will explore impacts of the characteristic SST pattern used in this study on precipitation across the wider Indian Ocean region.

Across Australia (Figs. 4c,d) the overall rainfall distribution, with wetter coastal regions especially along the northern and eastern coastline, and a very dry interior, is simulated well, although the contrast is weaker than observed. In particular, the increased rainfall in the tropical north extends too far inland, as can be seen in Fig. 6b of Meehl et al. (2006). Notwithstanding these shortcomings, the seasonal cycle with the associated

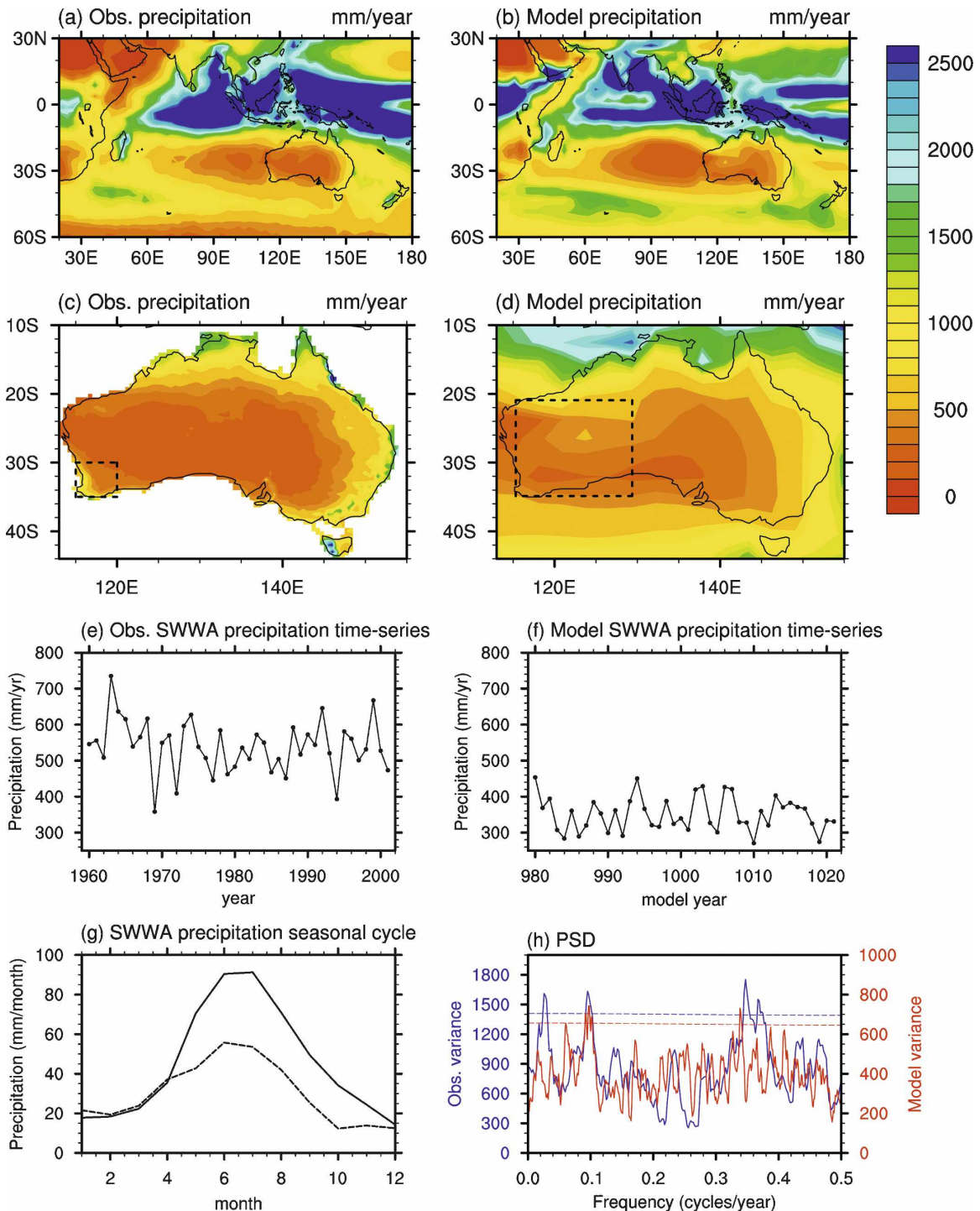


FIG. 4. Annual long-term mean of (a)–(d) rainfall (mm yr^{-1}) fields across (a), (b) the Indian Ocean basin and (c), (d) magnified over the Australian continent with the (left) observations and (right) model. The long-term mean in the observations in (a) is based on CMAP data for the 1979–2001 period, in (c) on the SILO data for 1960–2001, and in (b) and (d) on the model fields from the 80-yr control run (though for ease of comparison between observed and model, only the first 40 yr of the control are shown). The dashed box in (c) indicates the area used to derive the (e) observed and (f) model SWWA precipitation time series shown as annual values. The dashed box in (d) depicts the area termed WA. (g) The long-term seasonal cycle in precipitation for the observations (solid) and model (dashed). (h) The power spectral density shows the observed (model) variance for the dominant cycles in blue (red), with the dashed lines indicating a 95% confidence level according to white noise.

precipitation regimes across the Australian continent (i.e., winter rainfall in the south, summer monsoonal rainfall in the north) compare very favorably with observations (figure not shown). Despite a few regional rainfall deficiencies in the model, useful inferences can still be made regarding mechanisms for change in the simulations.

The time series for SWWA rainfall in the observations and the model (Figs. 4e,f) were derived for the region outlined by the boxes in Figs. 4c,d (for details also see section 2d). On average, the SWWA region records 540 mm yr^{-1} in the observations, while only 360 mm yr^{-1} are received in the model. The lower rainfall in the model is characteristic of climate models, considering its coarser resolution relative to the observations. The standard deviation of 74 mm yr^{-1} in the observations compares with 48 mm yr^{-1} in the model. However, a more appropriate metric of variability, the coefficient of variation (i.e., ratio of standard deviation and mean), demonstrates good agreement, with 0.137 and 0.133 for the observations and model, respectively. This indicates a comparable variability in SWWA rainfall on interannual time scales between observations and CAM3.

In line with the modeled annual mean precipitation, the amplitude of the seasonal cycle in the total precipitation is reduced over a large part of the year (May–November) in the model relative to the observations (Fig. 4g). However, the phase of the seasonal cycle with the majority of the rainfall falling in May–September is well reproduced. Model precipitation is given as the combination of stable large-scale and convective components. While the SILO dataset does not distinguish between these components, they are available as part of the NNR and are compared to the model components (figure not shown). For both the model and observations, the contribution of large-scale precipitation is considerably less than that resulting from convection. In the observations, convective rainfall occurs predominantly in winter (April–October), while it is more evenly distributed across the year in the model because of overestimated summer levels. The model large-scale precipitation in contrast is slightly higher than that observed throughout the year, though it reproduces the observed seasonal cycle of enhanced rainfall during April–August. Overall, the model has a higher proportion of total rainfall resulting from large-scale precipitation. Further investigation into the parameterization of precipitation in the model for convective and large-scale rainfall, and a detailed comparison with the NNR is beyond the scope of this study. Because broad features of the relative contribution of the two components and their seasonal cycle agree between the model

and observations, it seems reasonable to assume that the model is sufficiently realistic in terms of SWWA precipitation to be a useful tool to investigate precipitation characteristics. This is further suggested by a spectral analysis of SWWA rainfall showing coincident peaks in model and observed time series (Fig. 4h; peaks at 2–3 and 10 yr are significant at the 95% confidence level).

4. Seasonal evolution of the SST perturbation

The SST anomalies used in the perturbation experiments are based on characteristic observed SST patterns identified by England et al. (2006). The monthly varying SST anomalies averaged across their anomalous dry years in SWWA are shown in Fig. 1. They form the basis for the P_{DRY} run. England et al. (2006) found a characteristic tripole pattern in Indian Ocean SST [for the specific location of the poles see Fig. 5 in England et al. (2006)], consisting of one pole off the shelf to the northwest of Australia extending northwestward to Sumatra (P1; centered near 15°S , 120°E), a second pole of opposite polarity in the central subtropical Indian Ocean (P2; near 30°S , 100°E), and a third pole of the same sign as P1 to the southeast of Madagascar (P3; near 40°S , 50°E). In the remainder of the paper we will refer to those poles as P1, P2, and P3. This pattern gradually forms over the course of the year, becoming most prominent in late winter/early spring. Though not yet fully formed, the cold SST anomalies at P1 appear as early as January. In contrast, the warm anomalies at P2 are briefly revealed during January and February, but then weaken again until in May when they re-emerge and become a persistent feature. The anomalies in all three poles intensify until October. From November onward, anomalies in P1 decline, while the warm SST of P2 extends northward and covers the entire Indian Ocean north of 30°S by December. The seasonal evolution of the SST perturbation during P_{WET} shows a similar spatial and temporal development to P_{DRY} , with SST anomalies of opposite polarity (figure not shown).

It is of interest to compare the seasonal evolution of the pattern and magnitude of the composite SST anomalies used in the P_{DRY} simulation (Fig. 1) with the SST anomalies in a particular dry year in SWWA, namely 2006. The SWWA growing season (May–October) in 2006 was the driest ever recorded for many of the agricultural areas in Western Australia (DAFWA 2006). The SST anomalies of that specific dry year were not incorporated into the P_{DRY} forcing field, because only extreme years prior to 2003 were included in the England et al. (2006) composites. The seasonal evolution of SST anomalies in 2006 (Fig. 2)

broadly matches those in Fig. 1, both spatially and temporally, and in magnitude. In 2006, the SST anomalies at P1 and P2 intensified over the course of the year reaching maximum values of up to $\pm 1^\circ\text{C}$ in winter/early spring, which is of comparable magnitude to the perturbations in the same months (up to $\pm 1.2^\circ\text{C}$). The close match between the composite SST anomalies used as forcing and the 2006 SST anomalies demonstrates that the forcing is not of an unrealistically large magnitude. The use of the composite pattern for the forcing, rather than the pattern of a single year, allows more general inferences about other anomalous dry/wet years to be made. Similarly in 2005, a year with above-average precipitation across SWWA, the monthly SST anomalies across the Indian Ocean closely mirror the P_{WET} SST pattern (figures not shown), both temporally and spatially, and with anomalies of a comparable magnitude. This provides some limited evidence that the SST perturbations we apply represent a recurring SST pattern over the Indian Ocean. Correlation of the SWWA rainfall and Indian Ocean SST also reveals a qualitatively similar pattern with the three poles apparent (figure not shown). An empirical orthogonal function analysis of observed Indian Ocean SST (not shown) confirms this, with the second mode (the first mode represents the warming of the Indian Ocean) explaining 16% of the total variance in SST (Santoso 2005). This is of the same order of magnitude as the SST variance accounted for by the IOD (12%; Saji et al. 1999). The identification of the effects of this pattern on regional climate conditions is therefore of considerable importance.

As pointed out by England et al. (2006), the location and evolution of the poles in the Indian Ocean SST shown here (Figs. 1 and 2) are distinct from previous definitions of characteristic SST patterns, some of which have been linked to Australian rainfall. However, some similarities with previous SST patterns exist both in the tropics and subtropics of the Indian Ocean. The evolution of P1 in P_{DRY} is similar to the eastern pole of the tropical IOD shown by Saji et al. (1999) in their Fig. 2, especially in the second half of the year. The subtropical Indian Ocean dipole (SIOD) of Behera and Yamagata (2001) in their Fig. 4 is displaced to the west relative to our poles, with their warm SST anomalies located over the western edge of P2 and overlapping P3, and their cold pole to the west of P1 and less clearly defined. In addition, their SIOD SST anomalies reach their maximum earlier in the year (around February/March) compared to July–October in this study. The broad features of SST anomalies associated with the first rotated principal component of Australian an-

nual precipitation in Fig. 3 in Nicholls (1989) broadly agree with our P_{DRY} perturbation pattern (Fig. 1), though most closely during the August–October period. In light of the distinctiveness of our SST patterns from previous studies, both spatially and temporally, and their link to SWWA rainfall (England et al. 2006), it is of interest to explore the precipitation anomalies across western regions of Australia induced by these SST perturbations in an AGCM.

5. Precipitation changes

a. SWWA

We first assess the impact of the changed SST fields in the perturbation experiments on the rainfall distribution in the more limited SWWA region (Fig. 4c). The model rainfall distributions over SWWA across the ensemble members in P_{DRY} and P_{WET} relative to CNTRL are shown in Figs. 5 and 6, summed over different months. The model separates large-scale and convective precipitation, providing a first indication of likely causes in any shift in the rainfall distribution (based on all months) between P_{DRY} and P_{WET} . The large-scale annual rainfall distribution is shifted toward low (high) rainfall amounts for P_{DRY} (P_{WET}) relative to the CNTRL (both are significant at the 99% confidence level; see Figs. 5a,b). This is especially apparent at the upper end of the rainfall distribution for years receiving in excess of 150 mm yr^{-1} : while in the CNTRL case 8% of the years receive $150\text{--}170 \text{ mm yr}^{-1}$, none of the years in P_{DRY} record more than 150 mm yr^{-1} , but in 25% of the years in P_{WET} this threshold is passed (annual rainfall of $150\text{--}170 \text{ mm yr}^{-1}$ occurring in 13% of the years, $70\text{--}190 \text{ mm yr}^{-1}$ in 7%, and $190\text{--}210 \text{ mm yr}^{-1}$ in 5%). When focusing on the main rainfall season for SWWA, the period (May–September) during which 70% of the annual rainfall occurs, the same trends are observed, namely, a significant reduction (increase) is seen in the number of ensemble members receiving in excess of 100 mm of rainfall during May–September for the P_{DRY} (P_{WET}) case (Figs. 5c,d). For austral winter (June–August; Figs. 5e,f), only 5% of winters in the P_{DRY} case receive more than 65 mm, while this occurs in 9% of winters in the CNTRL and 32% in the P_{WET} case. Overall, a consistent shift in the large-scale annual and seasonal rainfall distribution is observed, with the upper end of the distribution losing (gaining) a disproportionate number of events for the dry (wet) cases.

The frequency distribution for convective rainfall over SWWA shows less consistent shifts (Fig. 6), with an apparent asymmetry between P_{DRY} and P_{WET} . An increase in the number of years with high convective

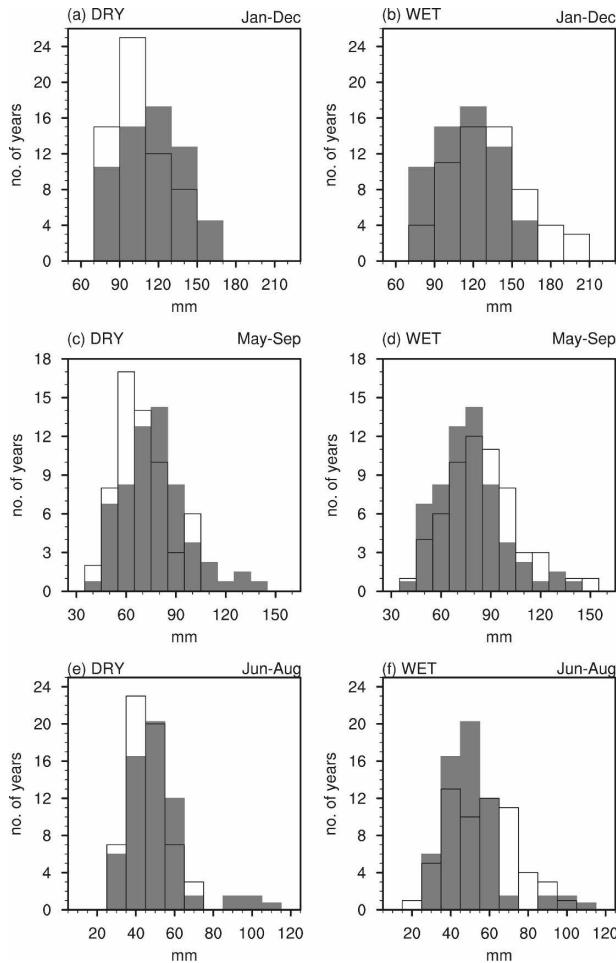


FIG. 5. Frequency distribution of large-scale rainfall spatially averaged across SWWA: rainfall amount (mm) summed for the months of (top) January–December, (middle) May–September, and (bottom) June–August for (left) P_{DRY} and (right) P_{WET} cases. The shaded gray rainfall distribution represents the CNTRL (normalized to the number of ensemble members in $P_{\text{DRY}}/P_{\text{WET}}$), while P_{DRY} and P_{WET} are indicated with black outlines. The following significance levels hold, as determined by a Mann–Whitney test: (a) 99%, (b) 99%, (c) 99%, (d) 95%, (e) 90%, and (f) 95%.

precipitation is observed for the P_{DRY} case (Figs. 6a,c,e). This trend is significant at the 99% confidence level for the January–December, May–September, and June–August periods. In contrast, the convective rainfall distribution for P_{WET} does not differ significantly from the CNTRL. A mechanism explaining this asymmetry, whereby the P_{DRY} forcing actually induces an *increase* in convective rainfall, will be proposed in section 6.

b. Western Australia

We focus now on a larger area across WA, excluding the tropical north of the state (see Fig. 4d). For this

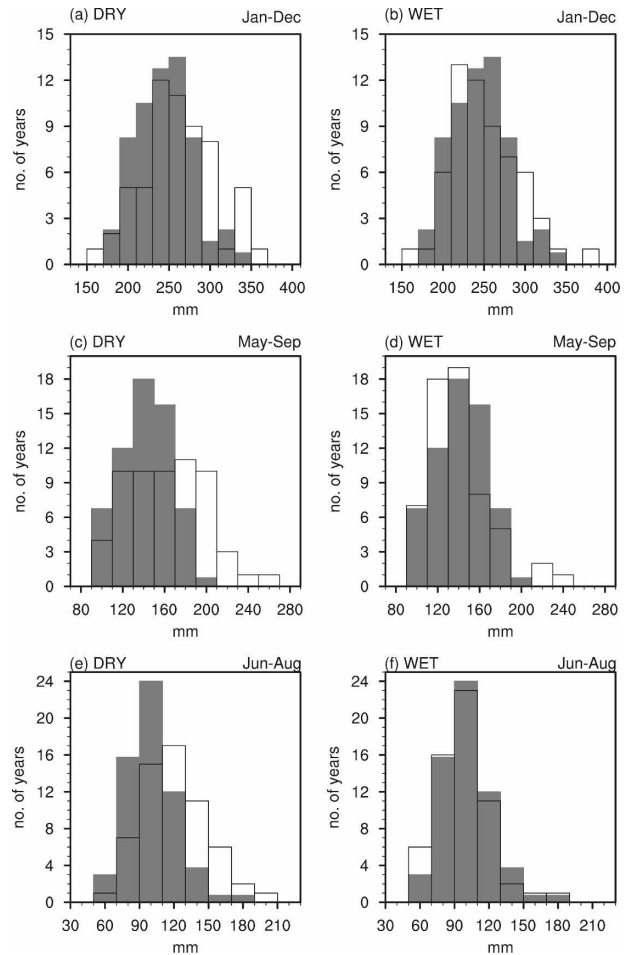


FIG. 6. Frequency distribution of convective rainfall spatially averaged across SWWA: rainfall amount (mm) summed for the months of (top) January–December, (middle) May–September, and (bottom) June–August for (left) P_{DRY} and (right) P_{WET} cases. The shaded gray rainfall distribution represents the CNTRL (normalized to the number of ensemble members in $P_{\text{DRY}}/P_{\text{WET}}$), while P_{DRY} and P_{WET} are indicated with black outlines. The following significance levels hold, as determined by a Mann–Whitney test (if nothing indicated, below 80%): (a) 99%, (c) 99%, (d) 80%, and (e) 99%.

larger region, shifts in rainfall distribution are evident for both the large-scale and convective precipitation and are of the same sign. Figure 7 presents the frequency distribution of total rainfall for WA. Now, the entire frequency distribution pattern for the annual total rainfall is clearly shifted toward lower (higher) rainfall amounts in the P_{DRY} (P_{WET}) case relative to the CNTRL (significant at the 99% confidence level; Figs. 7a,b). The shifts for the May–September and June–August are less prominent, though still significant as indicated (Figs. 7c–f). This can be attributed to the fact that as we extend the investigated area farther inland, we move from a region with predominant winter pre-

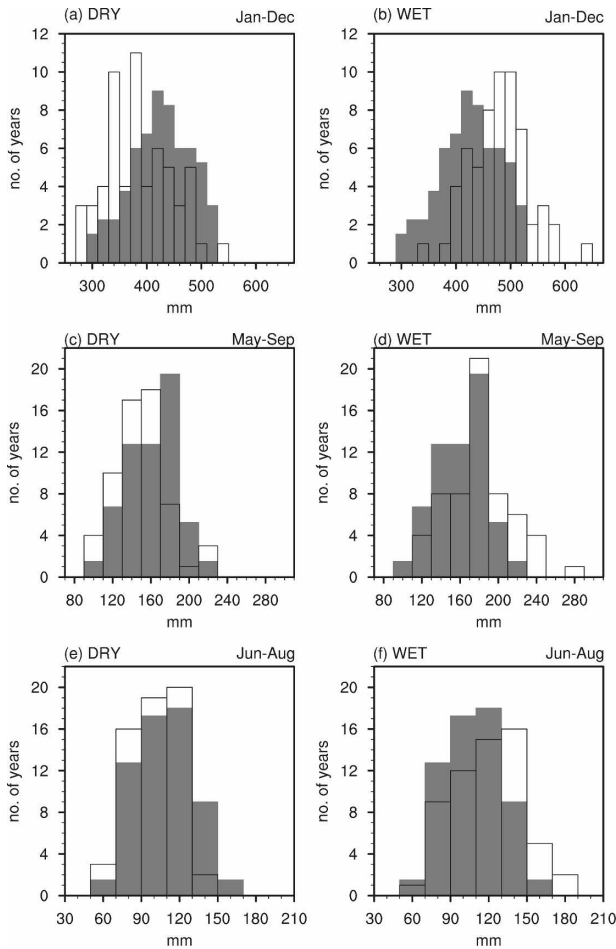


FIG. 7. Frequency distribution of total rainfall spatially averaged across Western Australia: rainfall amount (mm) summed for the months of (top) January–December, (middle) May–September, and (bottom) June–August for (left) P_{DRY} and (right) P_{WET} cases. The shaded gray rainfall distribution represents the CNTRL (normalized to the number of ensemble members in $P_{\text{DRY}}/P_{\text{WET}}$), while P_{DRY} and P_{WET} are indicated with black outlines. The following significance levels hold, as determined by a Mann–Whitney test: (a) 99%, (b) 99%, (c) 95%, (d) 99%, (e) 90%, and (f) 99%.

precipitation toward a more uniform distribution throughout the year. This means that the prominent shifts in annual rainfall distribution (Figs. 7a,b) are accumulated over the whole year. Furthermore, the opposing trends in convective and large-scale precipitation seen in SWWA are not apparent for the larger region WA. This relates most likely to the fact that with increasing distance inland, the impact of the warm SST at P2, giving rise to localized convective upward motion and enhanced convective rainfall in SWWA during P_{DRY} , is averaged away. The asymmetry in the convective rainfall over SWWA, not seen in the analysis for WA, will be investigated in more detail in section 6,

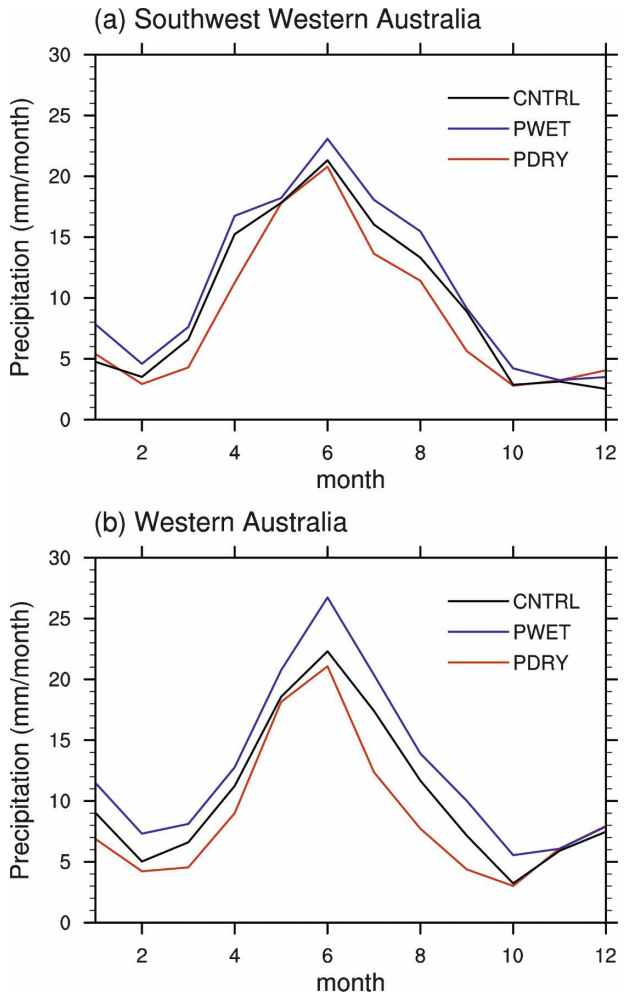


FIG. 8. Long-term seasonal cycle in model large-scale precipitation in the CNTRL (black), P_{DRY} (red), and P_{WET} (blue) runs over (a) SWWA and (b) Western Australia.

when the atmospheric dynamics leading to the changed rainfall distribution are explored.

c. Seasonal variability

The seasonal cycle in SWWA and WA rainfall in the perturbed cases is further investigated for the different rainfall types. The total monthly large-scale rainfall over each region is presented in Fig. 8, showing a notable reduction (increase) in P_{DRY} (P_{WET}). In contrast, when including convective events, the total rainfall (figure not shown) in P_{DRY} shows an intensification of the seasonal cycle with enhanced winter precipitation (May–August) and a reduction in autumn, relative to the CNTRL. This amplification of the seasonal cycle in P_{DRY} can be attributed to the positive (negative) changes in the convective winter (autumn) rainfall,

while the annual cycle in large-scale rainfall remains unchanged. In contrast, P_{WET} is characterized by slightly wetter conditions in both rainfall types throughout the year, particularly in summer and autumn. So, in the P_{DRY} case, a further enhancement of the predominant winter precipitation occurs, driven largely by an increase in convective rainfall, while the amplitude of the seasonal cycle in P_{WET} rainfall is reduced. As above, the seasonal cycle of SWWA large-scale precipitation in the perturbed cases overall follows the CNTRL (Fig. 8a), though with a notable reduction (increase) in P_{DRY} (P_{WET}). For WA, although the seasonal cycle for large-scale precipitation also remains unchanged in the perturbed cases relative to the CNTRL, the rainfall amounts in each month deviate considerably more from the CNTRL than for the smaller region of SWWA. That is, in all months prior to November the large-scale precipitation in P_{DRY} (P_{WET}) consistently lies below (above) the CNTRL fields (Fig. 8b).

6. Mechanisms and atmospheric dynamics

To understand the mechanism responsible for the observed local and regional rainfall changes we now investigate large-scale atmospheric anomalies. Both thermal properties and circulation characteristics are explored across the Indian Ocean and adjacent landmasses during the dry and wet ensemble of experiments.

a. Thermal anomalies in the atmosphere

The seasonal thickness anomalies in Fig. 9 provide a measure of the thermal properties in the lower atmosphere and resultant atmospheric flow. The seasonal evolution of the P_{DRY} thickness anomalies (Figs. 9a,c,e) follows the evolution of the underlying SST anomalies (Fig. 1). In concert with the cold SST anomalies, negative thickness anomalies occur over the eastern Indian Ocean, south of Australia, and across parts of Australia during the first 3 months of the year. Warm SST anomalies in the central subtropical Indian Ocean start establishing the characteristic dipole pattern (P1 and P2) from May onward (Fig. 9; although individual months are not shown). This is followed by the formation of a positive thickness anomaly extending from the central subtropical Indian Ocean across southern regions of Australia, including SWWA, from July onward. During the winter months until October, the pattern of negative, positive, and negative thickness anomalies across the Indian Ocean (extending from the

northeast toward the southwest), reflects the sign and positions of P1, P2, and P3 in SST anomalies, respectively. The combination of the three poles leads to an easterly anomaly in the thermal wind across the SWWA region. This would lead to a weakening of the subtropical jet that normally reaches peak strength during the winter months, resulting in weaker interactions with low pressure disturbances and cold fronts moving through the region. This could account for the reduction in large-scale rainfall during P_{DRY} and is particularly prominent during the winter months (Figs. 5c,e). The positive thickness anomaly over SWWA persists until October.

The development of the thickness anomalies during P_{WET} over the eastern Indian Ocean and Australia (Figs. 9b,d,f) is, on a broad scale, the reversal of the P_{DRY} evolution. Positive thickness anomalies dominate until April across the Indian Ocean region and Australia. Simultaneous with a strengthening of the P_{WET} SST dipole structure in May (figure not shown), warm thickness anomalies strengthen over the P1 location to the northwest of Australia. At the same time, cold thickness anomalies develop in the subtropical Indian Ocean off the coast of SWWA. The meridional gradient in thickness between the tropics (P1) and subtropics (P2) further intensifies over the following months. This represents an intensification of the underlying seasonal cycle. The intersecting line between positive and negative anomalies to the north and south, respectively, passes through SWWA, extending toward the southeast. It moves farther north in September, with negative anomalies covering all southern regions of Australia.

The monthly thickness anomalies in both P_{DRY} and P_{WET} show the greatest response in the May–September period when the majority (close to 75%) of the annual SWWA precipitation falls. Hence, for the remainder of this study, we will focus on the May–September months. The thermal structure through the atmosphere arising from the SST perturbations is shown in cross-sections at 32°S in Fig. 10 averaged over the May–September period. The characteristic structure of cold (warm) SST anomalies at P1, warm (cold) anomalies at P2, and cold (warm) anomalies at P3 for P_{DRY} (P_{WET}) is apparent (Figs. 10a,b). The location of the cross section at 32°S is indicated by the black line in Figs. 10a,b and directly traverses the center of P2, while also showing some influences of P3. The warm temperature anomalies at P2 in P_{DRY} penetrate to a height of more than 4 km (Fig. 10c), with the maximum increases in temperature below 2 km (about 800 hPa). In contrast, the cold anomalies at P2 in P_{WET} only reach to a height of 2 km and are capped by warm anomalies

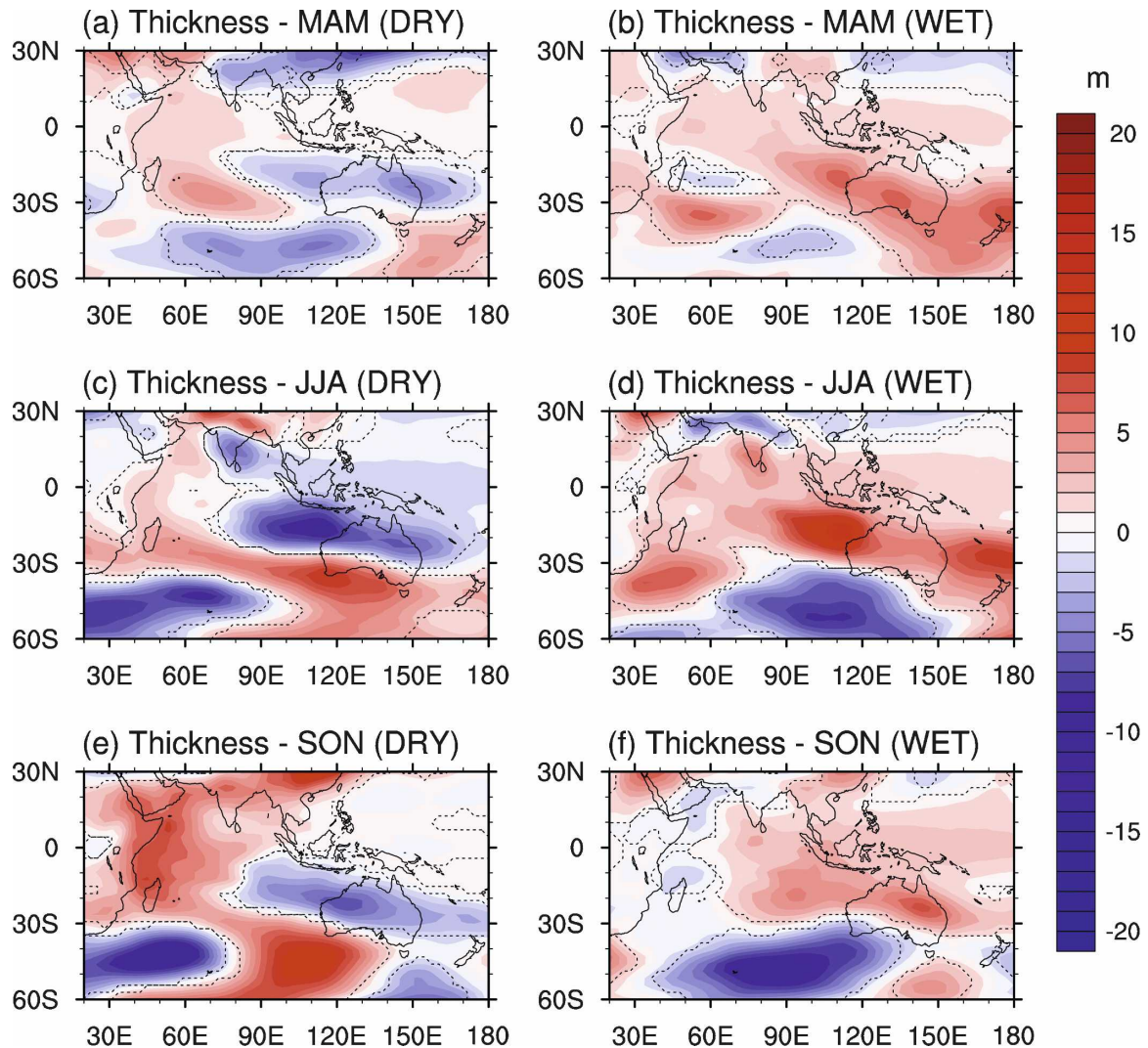


FIG. 9. Average seasonal thickness (m, for 1000–500 hPa) anomaly for (left) P_{DRY} and (right) P_{WET} , relative to the CNTRL for the (a), (b) March–May, (c), (d) June–August, and (e), (f) September–November seasons. Dashed lines indicate significant anomalies at the 90% confidence level as estimated by a two-tailed t test.

aloft (Fig. 10d). This asymmetry seems reasonable, because warm surface anomalies will produce a more unstable air column that has the ability to mix the warm air higher into the atmosphere than the cold anomalies. This may explain the increase in convective rainfall over SWWA seen in P_{DRY} (Fig. 6c), but not in P_{WET} (Fig. 6d), because the convective activity in the former would be stronger likely because of the enhanced temperature lapse rate through a deep atmospheric column. By way of contrast, the thermal structure in Fig. 10d seems more favorable for episodes of slow widespread ascent and associated rain, as warm, moist air is forced to move southward over the cold SST anomaly by an eastward-moving trough. The asymmetry may additionally affect circulation anomalies arising from

changes in the thermal properties of the atmosphere. This is investigated below.

b. Circulation anomalies in the atmosphere

Circulation anomalies in the atmosphere are shown in Fig. 11 for horizontal winds at 500 hPa and vertical velocity at 700 hPa during the May–September period for P_{DRY} and P_{WET} , respectively. Broadly speaking, anomalies in the horizontal winds relate to changes in the large-scale stable precipitation, while vertical velocity anomalies mostly are associated with convective rainfall. During P_{DRY} , there is a weakening of the anticyclonic circulation over the Indian Ocean basin (Fig. 11a). This is especially apparent in a reduction in the

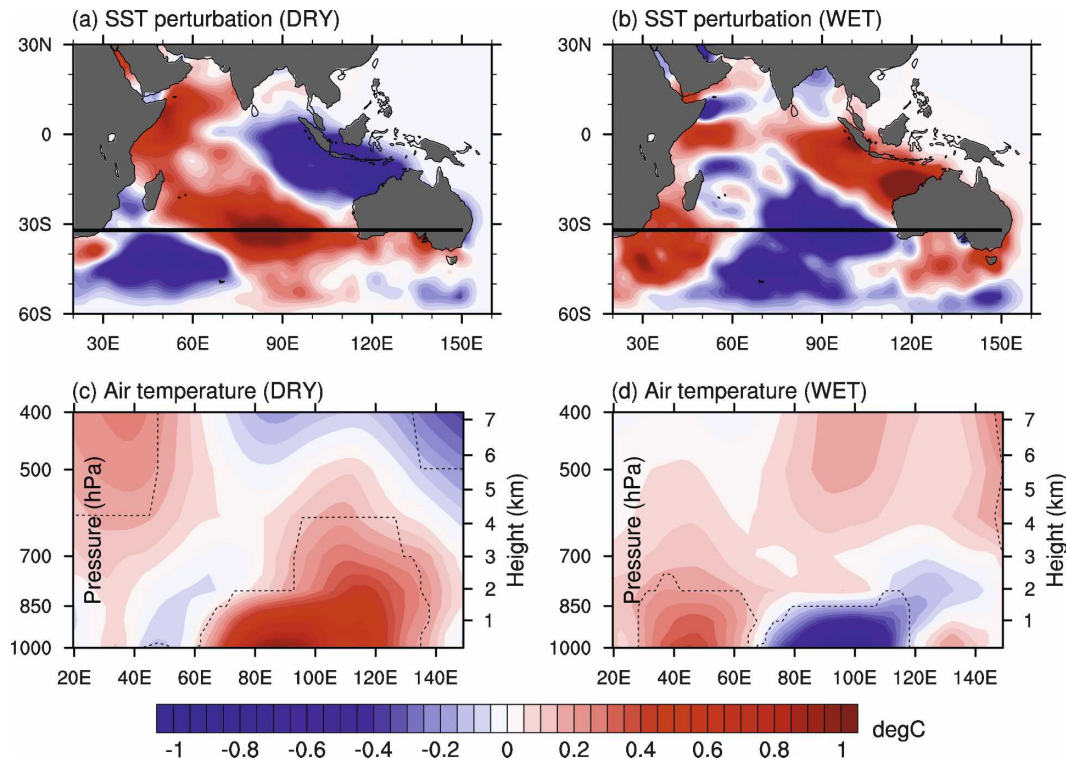


FIG. 10. (a), (b) SST perturbation and (c), (d) cross section of air temperature anomalies for the (left) P_{DRY} and (right) P_{WET} case averaged over the May–September period ($^{\circ}\text{C}$). The 32°S location of the cross section in (c), (d) is marked by black lines in (a), (b). Dashed lines in (c), (d) indicate significant anomalies at the 90% confidence level as estimated by a two-tailed *t* test.

easterly wind field over the eastern Indian Ocean at 10° – 20°S . Over southern regions of Australia, easterly anomalies occur as well, resulting in anomalous offshore flow over SWWA. In contrast during P_{WET} , enhanced onshore flow and westerly anomalies dominate over the Australian continent south of 20°S (Fig. 11b). The weakened (strengthened) onshore wind anomalies are consistent with the sign and position of the reduced (enhanced) gradient in thickness resulting from the underlying cold (warm) SST anomalies at P1 and warm (cold) anomalies at P2 during P_{DRY} (P_{WET}). The surface horizontal circulation anomalies induced by the SST perturbations in this study (figure not shown) closely mirror anomalous surface winds associated with dry/wet SWWA rainfall years in observations (England et al. 2006).

Significant anomalies in vertical velocity (Figs. 11c,d) are mainly confined to the tropics, being positive (negative) over the equatorial eastern Indian Ocean and parts of the Indonesian Archipelago during P_{DRY} (P_{WET}). This reduction (enhancement) in rising motion over the equatorial Indian Ocean during P_{DRY} (P_{WET}) is located above the underlying cold (warm) SST anomalies at P1. Significant vertical velocity anomalies

over the P2 pole occur in the P_{DRY} case only. This indicates a reduction in subsidence off the SWWA coast (Fig. 11c). Again, this helps to explain the significant increase in convective rainfall over SWWA for P_{DRY} (Fig. 6c), but not for P_{WET} (Fig. 6d).

A further indication of stability in the atmosphere is provided by the Eady growth rate, a measure of the baroclinic instability in the atmosphere. The Eady growth rate was calculated according to Paciorek et al. (2002), using the vertical gradient in horizontal wind speed and the Brunt–Väisälä frequency as a measure of static stability. It provides an indication of the development of low pressure systems (Risbey et al. 2007, manuscript submitted to *Int. J. Climatol.*), which are associated with increased rainfall. Mean states of the Eady growth rate in the model during winter (figure not shown) compare well with observations (e.g., Fig. 5 in Risbey et al. 2007, manuscript submitted to *Int. J. Climatol.*). During the May–September period in P_{DRY} , negative anomalies in Eady growth rate extending across southern regions of Australia indicate a reduction in baroclinicity and hence a lower formation rate of instabilities (Fig. 12a). An increase in instabilities is seen over northern regions of Australia and the eastern

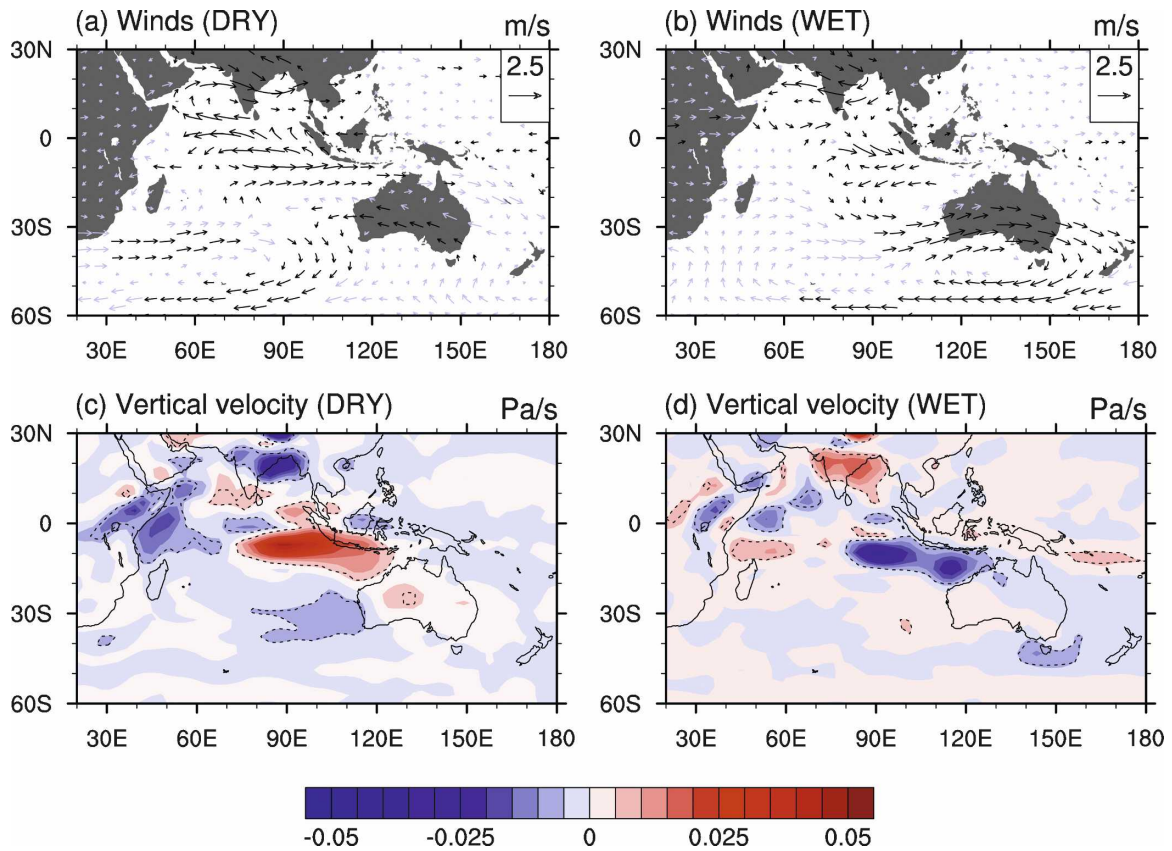


FIG. 11. Anomalies of (a), (b) winds at 500 hPa (m s^{-1}) and (c), (d) vertical velocity at 700 hPa (Pa s^{-1}) for the (left) P_{DRY} and (right) P_{WET} case averaged over the May–September period (positive, being downward). Black vectors in (a), (b) and dashed lines in (c), (d) indicate significant anomalies at the 90% confidence level as estimated by a two-tailed t test.

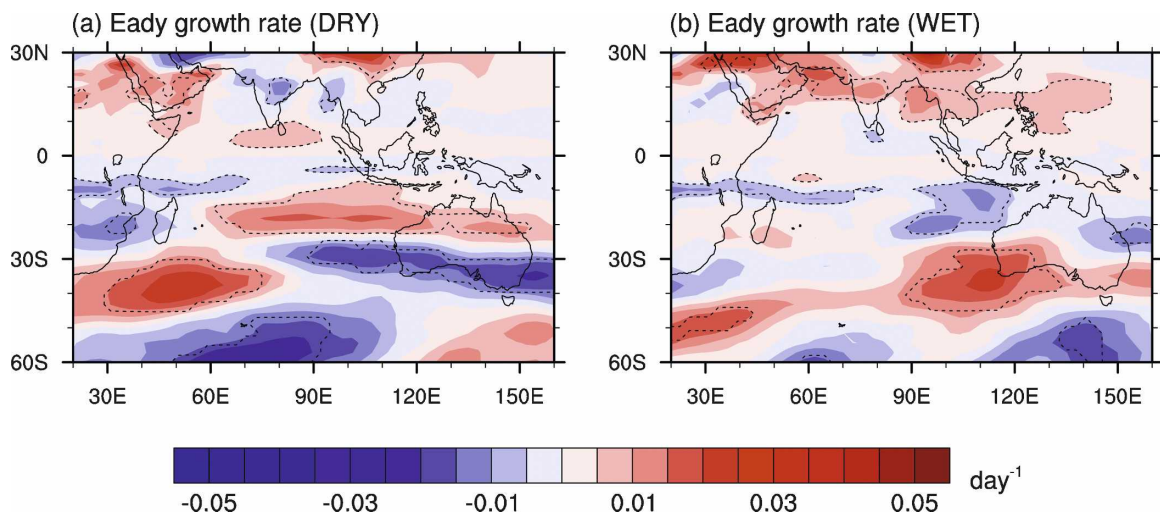


FIG. 12. Anomalies of Eady growth rate (day^{-1}) for the (a) P_{DRY} and (b) P_{WET} case averaged over the May–September period. Dashed lines indicate significant anomalies at the 90% confidence level as estimated by a two-tailed t test. Positive (negative) values indicate an increase (decrease) in baroclinicity and development of more (less) instabilities.

Indian Ocean over the 10° – 20° S latitude band, coinciding with the westerly wind anomalies there (Fig. 11a). The positive anomalies in Eady growth rate during P_{WET} are centered over SWWA and the adjacent Indian Ocean region, representing a local enhancement of baroclinicity with increased instabilities just offshore of SWWA (Fig. 12b). The location of the increased baroclinicity over the P2 cold SST anomalies during P_{WET} hints at their role in forcing the increased large-scale rainfall recorded over SWWA. In contrast, reduced instability is observed overlying the P1 region off the northwest shelf of Australia. Under an enhanced SST gradient in the eastern Indian Ocean reminiscent of the P_{WET} forcing, Frederiksen and Frederiksen (1996) find increased baroclinicity and an equatorward shift of storm-track instability modes over southern regions of Australia. This is consistent with the results presented here.

7. Summary and conclusions

In this study we have used AGCM simulations to assess the way Indian Ocean SST anomalies modulate midlatitude precipitation across southern and western regions of Australia. This represents an extension of previous work by England et al. (2006) who find extremes in SWWA rainfall associated with characteristic SST patterns and reorganization in the large-scale atmospheric circulation across the Indian Ocean. Here, we have presented evidence that these composite SST patterns significantly affect SWWA and WA precipitation in ensemble sets of AGCM simulations. We have also proposed a mechanism for the observed rainfall shifts resulting from changes in the large-scale general circulation.

Good agreement between the model mean fields and reanalysis data on annual and seasonal time scales indicates that the model represents the general atmospheric circulation across the Indian Ocean region suitably well. Over the Australian continent, the seasonal rainfall distribution associated with the monsoons in the north in summer and winter rainfall in the south of the country are well captured, though some regional biases exist (e.g., Meehl et al. 2006). Over the study region of SWWA, interannual variability and the seasonal cycle of the observed and model rainfall is comparable, although the long-term means in the model are lower than those observed. Despite certain biases in the model regarding tropical Pacific climate (e.g., Zhang and Wang 2006; Deser et al. 2006) and a slight enhancement of zonal flow at midlatitudes (Sen Gupta and

England 2006; Hurrell et al. 2006), the model performs sufficiently well over the Indian Ocean and Australian region to justify its use in the present study.

The monthly varying Indian Ocean SST composite patterns used as perturbations in the AGCM simulations appear to represent a realistic and recurring SST pattern (Santoso 2005). This is evidenced by the close match in the spatial and temporal evolution of the dry-year SST perturbation (Fig. 1) and the SST anomalies during 2006, which are not included in the composite fields (Fig. 2). The characteristic dipole pattern, which is distinct in location and temporal evolution from previous definitions of dipoles in the Indian Ocean (e.g., Saji et al. 1999; Behera and Yamagata 2001), develops with cold (warm) SST anomalies in the eastern Indian Ocean over the northwest shelf of Australia (P1) and warm (cold) anomalies in the central subtropical Indian Ocean (P2) during dry (wet) years in SWWA, reaching maximum values in late winter/early spring (Fig. 1).

Significant changes occur in the distribution of SWWA and WA precipitation in the perturbation experiments with the modified SST patterns (P_{DRY} and P_{WET}). In particular,

- 1) A consistent shift in winter and annual large-scale stable precipitation over SWWA is recorded, with the upper end of the distribution losing (gaining) a disproportionate number of events in P_{DRY} (P_{WET}).
- 2) An apparent asymmetry is seen in the response of winter and annual *convective* precipitation in SWWA, with an increase in P_{DRY} convective rainfall, while no significant changes are apparent in P_{WET} .
- 3) For WA, a shift of the entire rainfall distribution toward the low (high) end of the distribution is observed for P_{DRY} (P_{WET}), for both convective and large-scale precipitation.

To understand the mechanism(s) responsible for these rainfall changes, we investigated anomalies in thermal properties of the atmosphere and in the general circulation. Thickness anomalies of the same sign and position as the underlying SST anomalies at P1 and P2 develop in the perturbation experiments, intensifying toward late winter and extending across southern regions of Australia (Fig. 9). This leads to a weakening (intensification) of the meridional thickness gradient and the subtropical jet during the winter in P_{DRY} (P_{WET}), with a coincident easterly (westerly) anomaly in the thermal wind over southern regions of Australia. The anomalously offshore (onshore) winds over SWWA (Figs. 11a,b) could thus contribute to a reduc-

tion (increase) in large-scale rainfall. In the observed record, Ansell et al. (2000) similarly associate variations (and trends) in SWWA rainfall with modulations in the subtropical high pressure belt and a shift of the circum-polar trough. However in their study, links with Indian and Pacific Ocean SST are weak compared to the variability of the large-scale atmospheric circulation, while we demonstrate that the reorganization in the general atmospheric circulation arises as a *result* of the changed SST fields in the AGCM simulations.

A measure of the baroclinic stability in the atmosphere, and hence its disposition toward the development of rain-bearing low pressure systems, is provided by the Eady growth rate (Paciorek et al. 2002). A reduction (increase) in the Eady growth rate (Fig. 12) indicates a lower (higher) formation rate of baroclinic instabilities over southern and western regions of Australia during P_{DRY} (P_{WET}), consistent with the large-scale rainfall changes. Hope et al. (2006) also linked trends in baroclinicity and reduced frequency of passing troughs across the region with the observed rainfall decrease in SWWA. Similarly, Frederiksen and Frederiksen (2005, 2007) suggest that these decreases resulted from changes in the intensity and southward deflection of regions of cyclogenesis resulting from a decline in midlatitude baroclinicity. Over the Australian region, they find a 30% decrease in the growth rate of leading Southern Hemisphere cyclogenesis modes associated with a reduction in the vertical mean meridional temperature gradient, and in the peak upper-tropospheric jet stream zonal winds at 30°S. Here, we have demonstrated that such changes can be forced by anomalous SST patterns over the Indian Ocean.

The asymmetry in convective precipitation can be related to anomalies in the thermal properties of the atmosphere (Fig. 10), with the warm underlying SST at P2 during P_{DRY} penetrating higher into the atmosphere (resulting from an enhanced temperature lapse rate) than the cold P_{WET} anomalies. The vertical thermal structure in P_{DRY} thus could favor localized increases in convective activity, as seen in the increase in convective rainfall over SWWA and the reduction in large-scale rainfall. On the other hand, both the circulation and thermal anomalies in P_{WET} may enhance widespread ascent of moist air masses associated with frontal movement, as evidenced by increases in large-scale precipitation in that ensemble set.

Considering the significant drop in precipitation in SWWA since the 1970s (e.g., Allan and Haylock 1993; IOCI 2001; Timbal et al. 2006) and the projections for its continuation over the coming decades (Cai et al. 2003; Timbal 2004; Cai and Cowan 2006; Hope 2006), it

is of interest to relate our findings on interannual rainfall variations in SWWA to long-term trends. Recent changes in the large-scale Southern Hemisphere general circulation have been described in several studies. These include trends in the SAM toward its high-index phase (e.g., Li et al. 2005; Cai and Cowan 2006; Hendon et al. 2007), a consistent poleward shift in the zones of strong baroclinicity (Yin 2005), reductions in the density of low pressure systems (Smith et al. 2000), shifts in the subtropical jet (Frederiksen and Frederiksen 2005), and the reduced intensity of cyclogenesis (Frederiksen and Frederiksen 2005, 2007), among others. In this study, we have identified mechanisms by which these factors, driven by SST, modulate precipitation, both at a regional scale for SWWA and over interannual time scales. It is thus possible that the ocean plays a vital role in driving these atmospheric circulation changes that have led to longer-term trends in SWWA rainfall, especially as recent Indian Ocean SST trends favor a tendency toward the P_{DRY} thermal gradient (England et al. 2006). This is supported by other studies. For example, Smith et al. (2000) suggest that long-term SWWA rainfall variability is influenced by coupled air-sea interactions across the South Indian Ocean, linking SST and MSLP. Frederiksen and Balgovind (1994) demonstrated a connection between the frequency of northwest cloud bands and Indian Ocean SST gradients.

In summary, we have presented evidence that Indian Ocean SST is indeed instrumental in *forcing* midlatitude rainfall changes over regions of southern and western Australia. The characteristic SST pattern we investigate is thus not simply symptomatic of the changed wind field, but it could also play an important role in modulating the atmospheric circulation and rainfall anomalies. These findings are in contrast with some previous work on midlatitude rainfall in general (Kushnir et al. 2002, and references therein), and for the Australian region in particular (Watterson 2001, though his experiments do not employ a scaled SST forcing). We do not dispute the main hypothesis of Watterson (2001)—that interannual variations in seasonal rainfall are primarily driven by internal atmospheric mechanisms. However, this does not rule out the possibility of significant modulation by Indian Ocean SST forcing. Indeed Watterson (2001) refers to other GCM studies that find a proportion of the rainfall variance being explained by SST variability. Our results suggest a modest, yet significant, change in the frequency distribution for rainfall (i.e., the extreme events) resulting from SST anomalies, which is not necessarily captured by a total rainfall metric. It still remains an open ques-

tion as to what initially drives the formation of the characteristic SST anomaly pattern (e.g., internal ocean dynamics, ocean–atmosphere coupling), but this is beyond the scope of the present study and will be explored elsewhere. In a separate study, we will further investigate the implications of the present findings on improving predictability of SWWA rainfall. Considering the longer persistence of temperature anomalies in the ocean, as opposed to the higher-frequency variability in the atmosphere, we are hopeful that the mechanism presented here can help improve seasonal rainfall predictions, and thus ultimately aid in water management decisions in SWWA. In addition, the relative influence of the individual SST poles and the lead time of predictability warrant further investigation; these will be explored separately in a future study.

Acknowledgments. Use of the NCAR's CCSM3 model is gratefully acknowledged. The CMAP precipitation, NNR data, and NOAA_ERSST_V2 SST data were provided by NOAA/OAR/ESRL PSD, Boulder, Colorado, through their Web site (online at <http://www.cdc.noaa.gov>), and the ERA-40 data were provided by the ECMWF. The model simulations were run at the Australian Partnership for Advanced Computing National Facility. The manuscript benefitted from helpful discussions with Peter McIntosh and James Risbey, and comments by three anonymous reviewers. CCU was supported by the University of New South Wales under a University International Postgraduate Award, ASG and MHE by the Australian Research Council, and MJP partially by the Managing Climate Variability Program of Land and Water, Australia, and the CSIRO Wealth from Oceans National Research Flagship.

REFERENCES

- Allan, R. J., and M. R. Haylock, 1993: Circulation features associated with the winter rainfall decrease in Southwestern Australia. *J. Climate*, **6**, 1356–1367.
- Ansell, T. J., C. J. C. Reason, I. N. Smith, and K. Keay, 2000: Evidence for decadal variability in southern Australian rainfall and relationships with regional pressure and sea surface temperature. *Int. J. Climatol.*, **20**, 1113–1129.
- Arblaster, J. M., G. A. Meehl, and A. M. Moore, 2002: Interdecadal modulation of Australian rainfall. *Climate Dyn.*, **18**, 519–531.
- Ashok, K., Z. Guan, and T. Yamagata, 2003: Influence of the Indian Ocean Dipole on the Australian winter rainfall. *Geophys. Res. Lett.*, **30**, 1821, doi:10.1029/2003GL017926.
- Behera, S. K., and T. Yamagata, 2001: Subtropical SST dipole events in the southern Indian Ocean. *Geophys. Res. Lett.*, **28**, 327–330.
- Cai, W., and T. Cowan, 2006: SAM and regional rainfall in IPCC AR4 models: Can anthropogenic forcing account for southwest Western Australian winter rainfall reduction? *Geophys. Res. Lett.*, **33**, L24708, doi:10.1029/2006GL028037.
- , P. H. Whetton, and D. J. Karoly, 2003: The response of the Antarctic Oscillation to increasing and stabilized atmospheric CO₂. *J. Climate*, **16**, 1525–1538.
- Collins, W. D., and Coauthors, 2006: The Community Climate System Model version 3 (CCSM3). *J. Climate*, **19**, 2122–2143.
- Czaja, A., and C. Frankignoul, 1999: Influence of the North Atlantic SST on the atmospheric circulation. *Geophys. Res. Lett.*, **26**, 2969–2972.
- DAFWA, 2006: Seasonal update, November 2006. Department of Agriculture and Food, Government of Western Australia, 10 pp. [Available online at <http://www.agric.wa.gov.au/content/lwe/cli/seasonalupdatenov06.pdf>].
- Deser, C., A. Capotondi, R. Saravanan, and A. S. Phillips, 2006: Tropical Pacific and Atlantic climate variability in CCSM3. *J. Climate*, **19**, 2451–2481.
- Drosowsky, W., 1993: An analysis of Australian seasonal rainfall anomalies: 1950–1987. I: Spatial patterns. *Int. J. Climatol.*, **13**, 1–30.
- England, M. H., C. C. Ummerhofer, and A. Santoso, 2006: Interannual rainfall extremes over southwest Western Australia linked to Indian Ocean climate variability. *J. Climate*, **19**, 1948–1969.
- Frederiksen, C. S., and R. C. Balgovind, 1994: The influence of the Indian Ocean/Indonesian SST gradient on the Australian winter rainfall and circulation in an atmospheric GCM. *Quart. J. Roy. Meteor. Soc.*, **120**, 923–952.
- , and J. S. Frederiksen, 1996: A theoretical model of Australian Northwest cloudband disturbances and Southern Hemisphere storm tracks: The role of SST anomalies. *J. Atmos. Sci.*, **53**, 1410–1432.
- , and —, 2005: Mid-1970s changes in the Southern Hemisphere winter circulation. Indian Ocean Climate Initiative Stage 2: Report of Phase I Activity, Indian Ocean Climate Initiative, 7–11.
- , D. P. Rowell, R. C. Balgovind, and C. K. Folland, 1999: Multidecadal simulations of Australian rainfall variability: The role of SSTs. *J. Climate*, **12**, 357–379.
- Frederiksen, J. S., and C. S. Frederiksen, 2005: Decadal changes in Southern Hemisphere winter cyclogenesis. CSIRO Marine and Atmospheric Research Paper 002, 35 pp.
- , and —, 2007: Interdecadal changes in Southern Hemisphere winter storm track modes. *Tellus*, **59A**, 599–617.
- Gentilli, J., 1972: *Australian Climate Patterns*. Thomas Nelson, 285 pp.
- Hack, J. J., J. M. Caron, S. M. Yeager, K. W. Oleson, M. M. Holland, J. E. Truesdale, and P. J. Rasch, 2006: Simulation of the global hydrological cycle in the CCSM Community Atmosphere Model Version 3 (CAM3): Mean features. *J. Climate*, **19**, 2199–2221.
- Harzallah, A., and R. Sadourny, 1995: Internal versus SST-forced atmospheric variability as simulated by an atmospheric general circulation model. *J. Climate*, **8**, 474–495.
- Hendon, H. H., D. W. J. Thompson, and M. C. Wheeler, 2007: Australian rainfall and surface temperature variations asso-

- ciated with the Southern Hemisphere Annular Mode. *J. Climate*, **20**, 2452–2467.
- Hope, P. K., 2006: Projected future changes in synoptic systems influencing southwest Western Australia. *Climate Dyn.*, **26**, 765–780.
- , W. Drosowsky, and N. Nicholls, 2006: Shifts in the synoptic systems influencing southwest Western Australia. *Climate Dyn.*, **26**, 751–764.
- Hurrell, J. W., J. J. Hack, A. S. Phillips, J. Caron, and J. Yin, 2006: The dynamical simulation of the Community Atmosphere Model version 3 (CAM3). *J. Climate*, **19**, 2162–2183.
- IOCI, 2001: Second research report—Towards an understanding of climate variability in south western Australia. Second Research Phase of the Indian Ocean Climate Initiative, 204 pp.
- Jeffrey, S. J., J. O. Carter, K. B. Moodie, and A. R. Beswick, 2001: Using spatial interpolation to construct a comprehensive archive of Australian climate data. *Environ. Model. Softw.*, **16**, 309–330.
- Kalnay, E., and Coauthors, 1996: The NCEP/NCAR 40-Year Reanalysis Project. *Bull. Amer. Meteor. Soc.*, **77**, 437–471.
- Kiehl, J. T., and P. R. Gent, 2004: The Community Climate System Model, version 2. *J. Climate*, **17**, 3666–3682.
- Kistler, R., and Coauthors, 2001: The NCEP–NCAR 50-Year Reanalysis: Monthly means CD-ROM and documentation. *Bull. Amer. Meteor. Soc.*, **82**, 247–267.
- Kushnir, Y., W. A. Robinson, I. Blad, N. M. J. Hall, S. Peng, and R. Sutton, 2002: Atmospheric GCM response to extratropical SST anomalies: Synthesis and evaluation. *J. Climate*, **15**, 2233–2256.
- Li, Y., 2007: Changes of winter extreme rainfall over Southwest Western Australia and the linkage to the Southern Annular Mode. *Proc. 10th Int. Meeting on Statistical Climatology*, Beijing, China, Chinese Academy of Sciences, 15–16.
- , W. Cai, and E. P. Campbell, 2005: Statistical modeling of extreme rainfall in southwest Western Australia. *J. Climate*, **18**, 852–863.
- McIntosh, P. C., M. J. Pook, J. S. Risbey, S. N. Lisson, and M. Rebbeck, 2007: Seasonal climate forecasts for agriculture: Towards better understanding and value. *Field Crops Res.*, **104**, 130–138, doi:10.1016/j.fcr.2007.03.019.
- Meehl, G. A., and J. M. Arblaster, 1998: The Asian–Australian monsoon and El Niño–Southern Oscillation in the NCAR Climate System Model. *J. Climate*, **11**, 1356–1385.
- , —, D. M. Lawrence, A. Seth, E. K. Schneider, B. P. Kirtman, and D. Min, 2006: Monsoon regimes in the CCSM3. *J. Climate*, **19**, 2482–2495.
- Nagarajan, B., and A. R. Aiyer, 2004: Performance of the ECMWF operational analyses over the tropical Indian Ocean. *Mon. Wea. Rev.*, **132**, 2275–2282.
- Nicholls, N., 1989: Sea surface temperatures and Australian winter rainfall. *J. Climate*, **2**, 965–973.
- Paciorek, C. S., J. S. Risbey, V. Ventura, and R. D. Rosen, 2002: Multiple indices of Northern Hemisphere cyclone activity, winters 1949–99. *J. Climate*, **15**, 1573–1590.
- Pitman, A. J., G. T. Narisma, R. A. Pielke Sr., and N. J. Holbrook, 2004: Impact of land cover change on the climate of southwest Western Australia. *J. Geophys. Res.*, **109**, D18109, doi:10.1029/2003JD004347.
- Priestley, C. H. B., and A. J. Troup, 1966: Droughts and wet periods and their association with SST. *Aust. J. Sci.*, **29**, 56–57.
- Rayner, N. A., D. E. Parker, E. B. Horton, C. K. Folland, L. V. Alexander, D. P. Rowell, E. C. Kent, and A. Kaplan, 2003: Global analyses of sea surface temperature, sea ice, and night marine air temperature since the late nineteenth century. *J. Geophys. Res.*, **108**, 4407, doi:10.1029/2002JD002670.
- Rodwell, M. J., D. P. Rowell, and C. K. Folland, 1999: Oceanic forcing of the wintertime North Atlantic Oscillation and European climate. *Nature*, **398**, 320–323.
- Rowell, D. P., 1998: Assessing potential seasonal predictability with an ensemble of multidecadal GCM simulations. *J. Climate*, **11**, 109–120.
- Saji, N. H., B. N. Goswami, P. N. Vinayachandran, and T. Yamagata, 1999: A dipole mode in the tropical Indian Ocean. *Nature*, **401**, 360–363.
- Santoso, A., 2005: Evolution of climate anomalies and variability of Southern Ocean water masses on interannual to centennial timescales. Ph.D. thesis, University of New South Wales, 326 pp.
- Sen Gupta, A., and M. H. England, 2006: Coupled ocean–atmosphere–ice response to variations in the Southern Annular Mode. *J. Climate*, **19**, 4457–4486.
- Smith, I. N., P. McIntosh, T. J. Ansell, C. J. C. Reason, and K. McInnes, 2000: Southwest western Australian winter rainfall and its association with Indian Ocean climate variability. *Int. J. Climatol.*, **20**, 1913–1930.
- Smith, T., and R. Reynolds, 2003: Extended reconstruction of global sea surface temperatures based on COADS data (1854–1997). *J. Climate*, **16**, 1495–1510.
- , and —, 2004: Improved extended reconstruction of SST (1854–1997). *J. Climate*, **17**, 2466–2477.
- Sterl, A., and W. Hazeleger, 2005: The relative roles of tropical and extratropical forcing on atmospheric variability. *Geophys. Res. Lett.*, **32**, L18716, doi:10.1029/2005GL023757.
- Streten, N. A., 1981: Southern Hemisphere sea surface temperature variability and apparent associations with Australian rainfall. *J. Geophys. Res.*, **86** (C1), 485–497.
- , 1983: Extreme distributions of Australian annual rainfall in relation to sea surface temperature. *J. Climatol.*, **3**, 143–153.
- Timbal, B., 2004: Southwest Australia past and future rainfall trends. *Climate Res.*, **26**, 233–249.
- , and J. M. Arblaster, 2006: Land cover change as an additional forcing to explain the rainfall decline in the south west of Australia. *Geophys. Res. Lett.*, **33**, L07717, doi:10.1029/2005GL025361.
- , —, and S. Power, 2006: Attribution of the late-twentieth-century rainfall decline in southwest Australia. *J. Climate*, **19**, 2046–2062.
- Uppala, S. M., and Coauthors, 2005: The ERA-40 re-analysis. *Quart. J. Roy. Meteor. Soc.*, **131**, 2961–3012.
- Voice, M. E., and B. G. Hunt, 1984: A study of the dynamics of drought initiation using a global general circulation model. *J. Geophys. Res.*, **89**, 9504–9520.
- von Storch, H., and F. W. Zwiers, 1999: *Statistical Analysis in Climate Research*. Cambridge University Press, 484 pp.

- Watterson, I. G., 2001: Wind-induced rainfall and surface temperature anomalies in the Australian region. *J. Climate*, **14**, 1901–1922.
- Wright, P., 1974: Seasonal rainfall in southwestern Australia and the general circulation. *Mon. Wea. Rev.*, **102**, 219–232.
- Xie, P., and P. A. Arkin, 1996: Analyses of global monthly precipitation using gauge observations, satellite estimates, and numerical model predictions. *J. Climate*, **9**, 840–858.
- Yin, J. H., 2005: A consistent poleward shift of the storm tracks in simulations of 21st century climate. *Geophys. Res. Lett.*, **32**, L18701, doi:10.1029/2005GL023684.
- Zelle, H., G. J. van Oldenborgh, G. Burgers, and H. Dijkstra, 2005: El Niño and greenhouse warming: Results from ensemble simulations with the NCAR CCSM. *J. Climate*, **18**, 4669–4683.
- Zhang, G. J., and H. Wang, 2006: Toward mitigating the double ITCZ problem in NCAR CCSM3. *Geophys. Res. Lett.*, **33**, L06709, doi:10.1029/2005GL025229.
- Zhang, X., W. Lin, and M. Zhang, 2007: Toward understanding the double Intertropical Convergence Zone pathology in coupled ocean-atmosphere general circulation models. *J. Geophys. Res.*, **112**, D12102, doi:10.1029/2006JD007878.